Journal for ImmunoTherapy of Cancer

Synergistic therapeutic combination with a CAF inhibitor enhances CAR-NK-mediated cytotoxicity via reduction of CAF-released IL-6

Young Eun Lee,[1,2] Ga-Yeon Go,[1] Eun-Young Koh,[3] Han-Na Yoon,[1] Minkoo Seo,[4] Seung-Mo Hong,[5] Ji Hye Jeong,[3] Jin-Chul Kim,[6] Duck Cho,[7,8] Tae Sung Kim,[2] Song Cheol Kim,[9] Eunsung Jun,[3,9] Mihue Jang [1,10]

To cite: Lee YE, Go G-Y, Koh E-Y, *et al*. Synergistic therapeutic combination with a CAF inhibitor enhances CAR-NK-mediated cytotoxicity via reduction of CAF-released IL-6. *Journal for ImmunoTherapy of Cancer* 2023;**11**:e006130. doi:10.1136/jitc-2022-006130

► Additional supplemental material is published online only. To view, please visit the journal online (http://dx.doi.org/10.1136/jitc-2022-006130).

YEL, G-YG and E-YK contributed equally.

Accepted 06 February 2023

For numbered affiliations see end of article.

Correspondence to
Dr Mihue Jang;
mihue@kist.re.kr

Professor Song Cheol Kim;
drksc@amc.seoul.kr

Professor Eunsung Jun;
eungsungjun@amc.seoul.kr

ABSTRACT

Background Cancer-associated fibroblasts (CAFs) in the tumor microenvironment (TME) contribute to an impaired functionality of natural killer (NK) cells that have emerged as a promising therapeutic modality. The interaction between CAFs and NK cells within the TME exerts major inhibitory effects on immune responses, indicating CAF-targeted therapies as potential targets for effective NK-mediated cancer killing.

Methods To overcome CAF-induced NK dysfunction, we selected an antifibrotic drug, nintedanib, for synergistic therapeutic combination. To evaluate synergistic therapeutic efficacy, we established an in vitro 3D Capan2/patient-derived CAF spheroid model or in vivo mixed Capan2/CAF tumor xenograft model. The molecular mechanism of NK-mediated synergistic therapeutic combination with nintedanib was revealed through in vitro experiments. In vivo therapeutic combination efficacy was subsequently evaluated. Additionally, the expression score of target proteins was measured in patient-derived tumor sections by the immunohistochemical method.

Results Nintedanib blocked the platelet-derived growth factor receptor β (PDGFRβ) signaling pathway and diminished the activation and growth of CAFs, markedly reducing CAF-secreted IL-6. Moreover, coadministration of nintedanib improved the mesothelin (MSLN) targeting chimeric antigen receptor-NK-mediated tumor killing abilities in CAF/tumor spheroids or a xenograft model. The synergistic combination resulted in intense NK infiltration in vivo. Nintedanib alone exerted no effects, whereas blockade of IL-6 trans-signaling ameliorated the function of NK cells. The combination of the expression of MSLN and the PDGFRβ$^+$-CAF population area, a potential prognostic/therapeutic marker, was associated with inferior clinical outcomes.

Conclusion Our strategy against PDGFRβ$^+$-CAF-containing pancreatic cancer allows improvements in the therapy of pancreatic ductal adenocarcinoma.

WHAT IS ALREADY KNOWN ON THIS TOPIC

⇒ NK cells have emerged as a promising therapeutic modality for cancer immunotherapy, as they play a key role in recognizing and killing various types of cancers cells in the first-line defense. Despite the benefits in harnessing NK cells for cancer treatment, cancer-associated fibroblasts (CAFs)in the tumor microenvironment contribute to the impaired functionality of NK cells. Particularly, CAF-secreted soluble mediators interfere with NK-mediated tumor killing, leading to a poor therapeutic response against cancers. While numerous combinations of CAF-targeting agents with immunotherapies have been developed until now, however, there are still challenges for overcoming the CAF-mediated immunosuppressive effects on NK cells.

WHAT THIS STUDY ADDS

⇒ Wediscovered that in PDGFRβ$^+$ CAFs, high amounts of IL-6 were secreted via PDGFRβ-mediated signal transduction; consequently, paracrine IL-6 attenuated the NKcytotoxic function through inhibition of pSTAT3-mediated activating receptors. Furthermore, we revealed that nintedanib inhibited CAF-derived IL-6, rescued NK function, and showed significantly enhanced tumor killing efficacy*in vitro* and *in vivo*.

HOW THIS STUDY MIGHT AFFECT RESEARCH, PRACTICE OR POLICY

⇒ Based on our work, the combination of expression of MSLN and the PDGFRβ$^+$ population, as well as the combination of expression of MSLN and the IL-6$^+$population, wereinvolved in unfavorable clinical outcomes with poor overall survival in PDAC. Therefore, our novel combination of MSLN-targeted CAR-NK and nintedanibcould provide a promising therapeutic option for the treatment of patients with PDAC tumors.

BACKGROUND

Pancreatic ductal adenocarcinoma (PDAC) is a devastating lethal malignancy with limited available therapeutic options.[1] PDAC features a massive desmoplastic stroma with a mixture of cancer cells, cancer-associated fibroblasts (CAFs), extracellular matrix (ECM) proteins, endothelial cells, and immune

cells.[2 3] Along with ECM remodeling, tumor stiffness, and chemoresistance, CAFs are major immunosuppressive players contributing to tumor progression and metastasis.[4 5] CAFs are highly involved in immune evasion by promoting the secretion of various immunosuppressive molecules such as cytokines, chemokines, and growth factors[6–8] and CAFs influence the infiltration, phenotype, and function of immune cells within the tumor microenvironment (TME) directly or indirectly.[9 10] CAFs in PDAC are a heterogeneous stromal population, sorted into three major distinct subtypes with different roles in tumor progression and immunity[11–13]; myofibrotic CAFs (myCAFs), inflammatory CAFs (iCAFs), and antigen presenting CAFs (apCAFs).[14 15] Among them, myCAFs exhibit a matrix-producing contractile phenotype with high expression of alpha-smooth muscle actin (α-SMA) and low expression of interleukin (IL)-6, whereas iCAFs show elevated expression of IL-6 along with an immunomodulating secretome. Despite the distinct CAF subtypes with different molecular markers, myCAFs and iCAFs are dynamically interconvertible according to their location and microenvironment cues.[16] Apart from classical myCAFs and iCAFs, apCAFs show antigen-presenting capacities.

Natural killer (NK) cells are cytotoxic effector cells that are able to diminish damaged, virus-infected, or malignant cells, independent of antigen processing and presentation.[17 18] NK cells play critical roles in tumor immunosurveillance, triggering antimetastatic functions through multiple killing mechanisms. Moreover, allogeneic NK cells, which are critically beneficial to the manufacturing process, allow their clinically scalable 'off-the-shelf' production without an additional gene editing process.[19 20] Despite the benefits in harnessing NK cells for solid cancer treatment, CAF-secreted soluble mediators such as IL-6, prostaglandin E_2 (PGE_2), indoleamine-pyrrole 2,3-dioxygenase (IDO), matrix metalloproteinases, and transforming growth factor-β (TGF-β) interfere with NK-mediated tumor killing, exerting poor therapeutic response against cancers.[21 22] For instance, CAF-driven PGE_2 paracrinally suppresses the expression of NK activating receptors, NKp44, NKp30, and NKG2D, resulting in the functional impairment of NK cells.[21] In a TGF-β-dependent manner, high levels of CAF-secreted IL-6 promote PDAC metastasis via STAT3 activation and induction of NK dysfunction.[23] Thus, the direct or indirect interaction between CAFs and NK cells within the TME exerts major inhibitory effects on immune responses, indicating CAF-targeted therapies as potential targets for effective cancer treatment.

Anti-CAF therapies have been accessed by augmenting antitumor immunity, including many approaches that target classical CAF markers, intracellular signaling components, and chemokine ligand-receptor axis.[24] Primarily, the direct depletion of a CAF subset has been attempted by targeting specific surface markers in various ways. For instance, genetic depletion of fibroblast-activation protein (FAP) exhibited reduced tumor progression, causing rapid hypoxic necrosis of both cancer and stromal cells, and TME modulation.[25] Likewise, elimination of FAP^+ CAFs by DNA vaccination or FAP-reactive chimeric antigen receptor (CAR)-T cells was accompanied by increased infiltration of $CD8^+$ T cells within the TME, improving anticancer efficacy.[26–28] Besides CAF-depleting approaches, recent studies have explored the effects of combinations of drugs targeting CAF activation pathways or CAF-derived molecules.[29] For example, administration of AMD3100, a chemokine receptor antagonist targeting the CXCL12-CXCR4 axis diminished FAP^+ CAF-mediated immunosuppression via the induction of rapid T cell accumulation and acted synergistically with anti-PD-L1 immunotherapy.[29] Accordingly, anti-CAF therapies influence the infiltration of cytotoxic immune cells with therapeutic benefits, ultimately dictating the success of immunotherapies. Despite the development of numerous combinations of CAF-targeting agents with immunotherapies, there are still challenges for overcoming CAF-mediated immunosuppressive effects on NK cells. Therefore, in this study, we investigated a promising therapeutic combination to improve NK-mediated cytotoxicity through the effective depletion of CAFs.

METHODS

In vivo studies

All animal care and experiments were performed according to the guidelines of the Institutional Animal Care and Use Committees of KIST (KIST-2020-049). For in vivo experiments, Capan2-Luc cells at a density of 2×10^6 cells or a mixture of Capan2-Luc cells and CAF cells at a 2:1 ratio were subcutaneously injected into each mouse. When tumors reached an average volume of 100 mm^3, mice were randomly divided into six groups and treated under various conditions. Tumor-bearing mice were administrated three times with 1×10^7 CAR-NK cells or 2 mg/kg nintedanib or both per mice. CAR-NK cells or nintedanib were intravenously or orally administrated, respectively. Tumor sizes were measured regularly using a caliper, and tumor volumes were calculated as length×$(\text{width})^2\times0.5$. To visualize Capan2-Luc tumor cells, in vivo luciferase images in isoflurane-anesthetized mice were obtained by intravenous injection of a substrate solution (Promega) using an IVIS spectrum imaging system (Perkin-Elmer, Norwalk, Connecticut, USA). Tumors and other normal organs of mice were scarified and paraffin-embedded blocks were prepared for further experiment.

For histological observation, H&E staining was performed in deparaffinized sections according to general procedures. Formalin-fixed, paraffin-embedded tissue sections were immunohistochemically stained for anti-IL-6 (1:800, cat no. ab6672, abcam), anti-mesothelin (MSLN) (1:80, clone 5B2, cat no. MA511918, Invitrogen, Carlsbad, California, USA), anti-platelet-derived growth factor receptor β (PDGFRβ) (1:200, clone L48, cat no. BS1290, Bioworld, St Louis, Missouri, USA) and

anti-CD56 (1:100, clone CD564, cat no. NCL-L-CD56-504, Novocastra, Leica Biosystems, Illinois, USA) using an OptiView DAB immunohistochemical (IHC) Detection Kit on a BenchMark XT automatic immunostaining device (Ventana Medical Systems, Tucson, Arizona, USA) according to the manufacturer's instructions. IL-6, MSLN, PDGFRβ, and CD56 staining images were scanned using a vs200 Research Slide Scanner (Olympus) and analyzed using the HALO platform (V.3.1.1076, Indica Labs, New Mexico, USA).

Clinicopathological characteristics of patients

Each patient had a follow-up period of at least 5 years, and medical records were retrospectively reviewed for clinicopathological characteristics including age, sex, operation method and pathological findings (tumor size, tumor differentiation, T stage, and N stage). Survival analysis using the Kaplan-Meier method with the log-rank test was performed using the SPSS V.21.0 (IBM).

IHC staining and scoring in human tissues

Pancreatic, gastric, and liver cancer tissues that were pathologically diagnosed as carcinoma were delivered from the Bio-resource center (BRC No. 2018-13(167)). For histological analysis, H&E staining was performed in deparaffinized sections according to general procedures. Formalin-fixed, paraffin-embedded tissue sections were immunohistochemically stained for anti-PDGFRβ (1:200, clone Y92, cat no. 1469-1, Epitomics, California, USA), anti-MSLN (1:20, clone 5B2, cat no. MA5-11918, Invitrogen), and anti-IL-6 (1:50, cat no. ab6672, Abcam, Cambridge, UK) using an OptiView DAB IHC Detection Kit on a BenchMark XT automatic immunostaining device (Ventana Medical Systems, Tucson, Arizona, USA) according to the manufacturer's instructions. A pathologist specialized in pancreatic cancer reviewed the slides and scored the degree of staining intensity from 0 to 3. PDGFRβ and IL-6 staining images were scanned using a vs200 Research Slide Scanner (Olympus) and analyzed using the HALO platform (V.3.1.1076, Indica Labs, New Mexico, USA).

RESULTS

Nintedanib, an antifibrotic drug that preferentially targets PDGFRβ, inhibited the proliferation of patient-derived PDAC CAFs

To select an antifibrotic drug as a promising candidate for combinatorial treatment in NK-mediated immunotherapy, we tested three chemical drugs that can attenuate pulmonary fibrosis: nintedanib, SOM230, and metformin.[30] FDA-approved nintedanib is a triple-angiokinase inhibitor that blocks the tyrosine kinase activities of fibroblast growth factor receptor (FGFR), vascular endothelial growth factor receptor (VEGFR), and PDGFR.[31 32] SOM230, a somatostatin analog, binds somatostatin receptors and inhibits collagen deposition via reduced expression of profibrotic mediators such as TGF-β and connective tissue growth factor.[33 34] Metformin used for the treatment of type 2 diabetes is a potent adenosine monophosphate-activated protein kinase (AMPK) activator that also reduces TGF-β-induced fibrosis.[35 36] Accordingly, to test their antifibrotic function, we evaluated the viability of patient-derived PDAC CAFs in the presence of nintedanib, SOM230, and metformin, respectively, in a dose-dependent manner (figure 1A). We tested each of the five types of CAFs isolated from fresh PDAC specimens (online supplemental figure S1 and table S1). Intriguingly, we observed that treatment with nintedanib led to a reduced growth of CAFs with half inhibitory concentration (IC)$_{50}$ values ranging from 9.76 to 40.84 µM, depending on the CAF subtype. Likewise, we found that treatment with nintedanib resulted in a gradual decrease in the expression of classical CAF markers, such as FAP and α-SMA, and was associated with an increment in cell death (figure 1B–D). To unveil the molecular targets of nintedanib in patient-derived PDAC CAFs, we evaluated the phosphorylation status of three putative targets, including PDGFRβ, VEGFR2, and FGFR1 in the presence of nintedanib (figure 1E). We detected that nintedanib mainly inhibited the PDGFRβ-mediated signaling pathway in CAFs with strong reduction of pPDGFRβ expression (figure 1E). We confirmed that treatment of nintedanib inhibited PDGF ligand-induced CAF proliferation (figure 1F). Furthermore, PDGFβ knock-out (K.O) CAFs had a minor effect on cellular cell death under nintedanib treatment (figure 1G,H).

Nintedanib preferentially inhibited the proliferation of CAFs compared with that of cancer cells via PI3K/AKT and MAPK/ERK signal pathways

To test the inhibitory effect of nintedanib on cancer cells, we treated PDAC cancer cells, including MIA PaCa-2 and Capan2, with nintedanib in a dose-dependent manner (figure 2A). Interestingly, we observed that nintedanib showed moderated inhibition of the viability of cancer cells compared with that of CAFs (figures 1A and 2A). Moreover, we detected that two major PDGF-mediated PI3K and MAP kinase signaling pathways were strongly inhibited in CAFs but not in Capan2 cancer cells, suggesting the prominent inhibitory effects of nintedanib on CAFs (figure 2B). We also found that nintedanib-treated CAFs exhibited a dose-dependent decrease in the phosphorylation of both AKT and ERK. We further confirmed the prominent inhibitory effects of nintedanib in CAFs in a Capan2-CAF coculture spheroid system using live cell imaging (figure 2C). When we produced cancer spheroids without CAFs using four different PDAC cell lines (Capan2, AsPC-1, PANC-1, and MIA PaCa-2), we detected that Capan2 cells formed regular and round-shaped spheroids with strong expression of collagen I (online supplemental figure S2). Hereafter, we used Capan2 cells for further experiments. For visualization, we transduced the expression of a GFP- and RFP-encoding genes in Capan2 and CAF cells, respectively. As expected, we found that CAFs were significantly reduced in spheroid

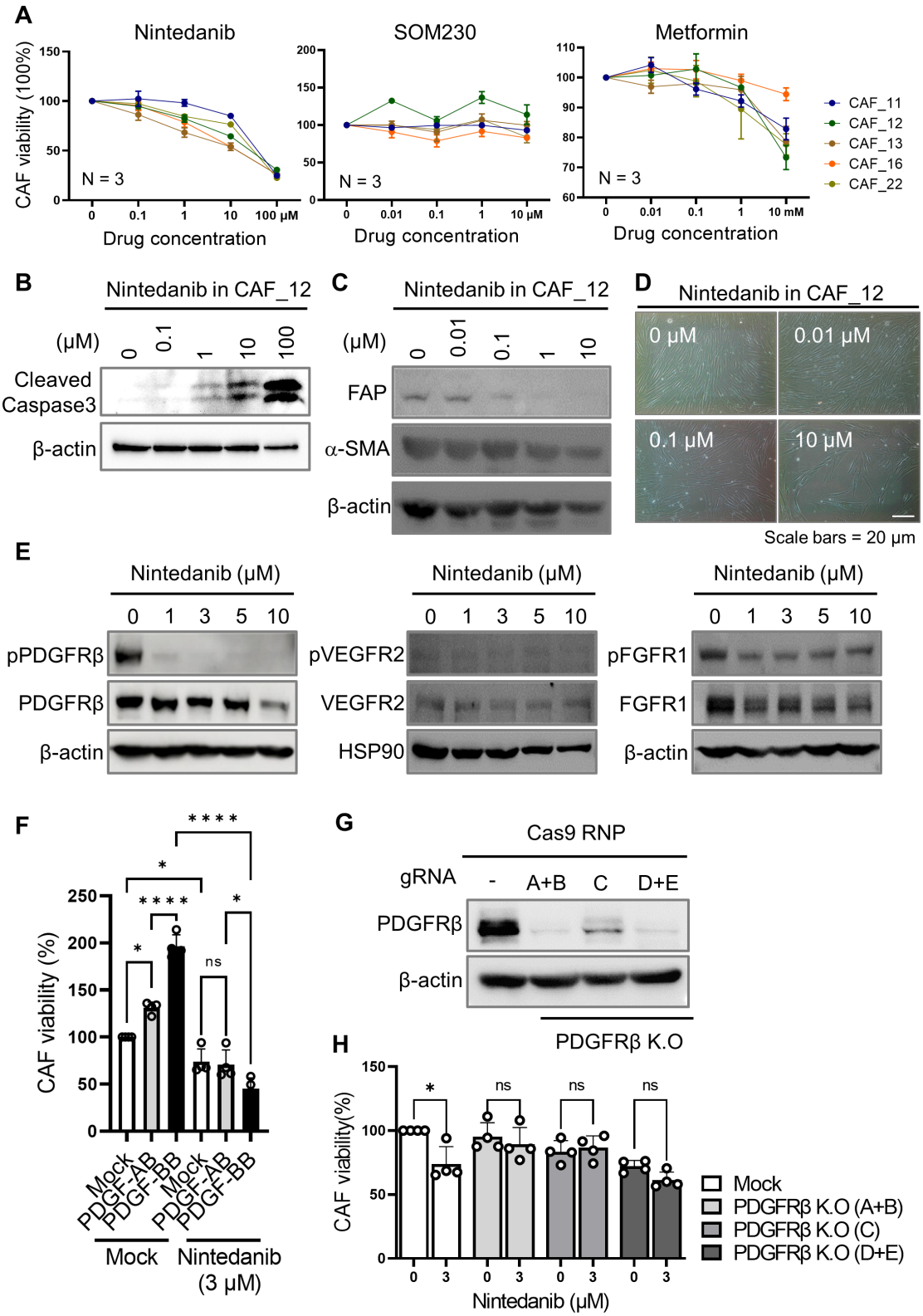

Figure 1 The selection of an antifibrotic drug for the depletion of patient-derived CAFs. (A) Cell viability was evaluated in five CAFs derived from patients with PDAC under treatment with nintedanib, SOM230, and metformin, respectively, as potential CAF-inhibiting drugs. Data were obtained from N=3 per each group. (B) Nintedanib-induced CAF cell death was validated by the level of cleaved caspase-3 using western blot experiments. (C) Nintedanib in CAF_12 lowered the expression of classical CAF markers in a dose-dependent manner. (D) Nintedanib-induced CAF cell death was observed using an optical microscope. (E) Putative molecular targets in response to nintedanib were accessed using western blot analysis. (F) The viability of CAF_12 in response to treatment with PDGF ligands was tested in the presence or absence of nintedanib. (*p<0.05, ****p<0.0001) (G, H) Nintedanib-induced CAF cell death was not affected in PDGFRβ K.O CAF cells achieved using CRISPR/Cas9.(*p<0.05) CAF, cancer-associated fibroblast; PDAC, pancreatic ductal adenocarcinoma; PDGFRβ, platelet-derived growth factor receptor β.

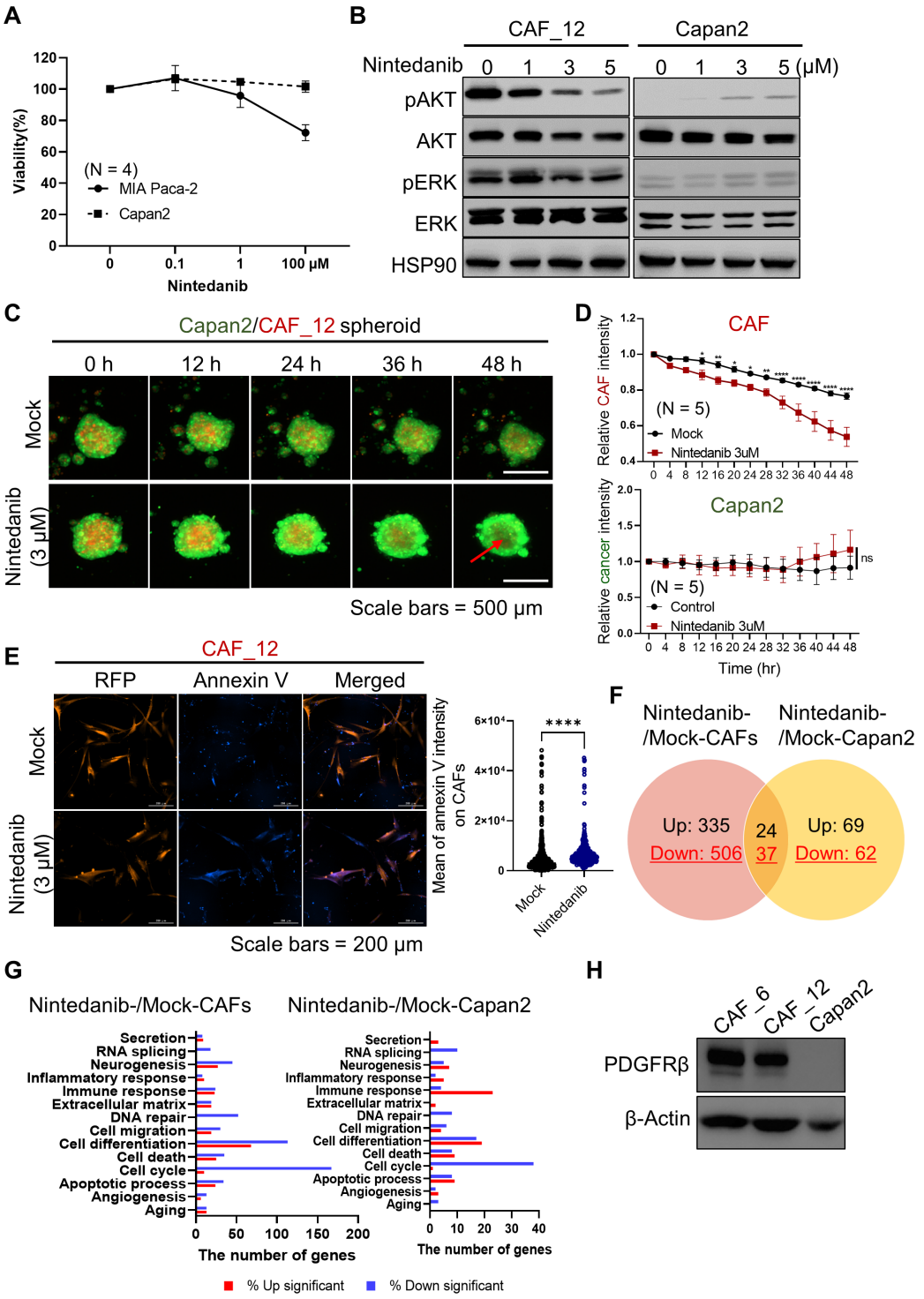

Figure 2 Prominent inhibitory effect of nintedanib in PDAC CAFs compared with cancer cells. (A) Cell viability was evaluated in cancer cells under treatment with nintedanib. (B) Nintedanib-treated CAFs exhibited decreased phosphorylation of AKT and ERK, members of the two major PDGF-mediated signaling pathways. Representative images were shown from one of three independent experiments. (C, D) Using a Capan2-CAF coculture spheroid system, live cell imaging was conducted in the presence or absence of nintedanib. Prior to coculture, GFP and RFP were introduced into Capan2 and CAF_12, respectively, for visualization. Quantitative data were obtained from N=5 per each group. P values were determined using one-way ANOVA followed by multiple comparison test. (*p<0.05, **p<0.01, ***p<0.001, ****p<0.0001) (E) Annexin V influx was measured on RFP expressing CAF cells to determine apoptotic death. Images from mock (N=861) and nintedanib (N=487) groups were visualized 24 hours post-treatment. P values were analyzed statistically using the unfired t-test. (****p<0.0001) (F, G) 3 μM nintedanib was added in CAF and Capan2, and then transcriptomic analysis was conducted in each sample (N=2). The number of differentially expressed genes (DEGs) with a fold change (FC) ≥2 and p<0.05 is shown in Venn diagram (F). The number of DEGs according to gene ontology enrichment (G). (H) Total expression of PDGFRβ on CAFs and Capan2 was accessed by a western blot experiment. ANOVA, analysis of variance; CAF, cancer-associated fibroblast; PDGFRβ, platelet-derived growth factor receptor β.

co-cultures in the presence of nintedanib, as indicated by the relative signal intensity (figure 2D). We further investigated whether the fluorescence signal reduction in CAFs under nintedanib treatment was associated with cell death of CAFs by measurement of annexin V influx in the dead cells (figure 2E). An increase in the annexin V signal inversely correlated with a decrease in the RFP signal from CAFs.

Consistent with our observations using live cell imaging, next-generation sequencing (NGS) revealed that the CAF group (nintedanib-treated CAFs vs mock-treated CAFs) had 902 differentially expressed genes (DEGs) with a fold change (FC)≥2 and p<0.05, whereas the cancer group (nintedanib-treated Capan2 vs mock-treated Capan2) had 192 DEGs (figure 2F). In particular, we found that the DEGs in the CAF group, which were involved in cell cycle, DNA repair, and cell death, were significantly down-regulated compared with those in the cancer group, indicating the prominent effect of nintedanib on CAFs (figure 2G). Additionally, we revealed that CAFs had a stronger expression of PDGFRβ than of Capan2, showing the preferential inhibitory effect of nintedanib on CAFs (figure 2H and online supplemental figure S3).

Nintedanib ameliorated NK-mediated cytotoxicity with elevated expression of activating receptors against cancer

Given the CAF-depleting effects of nintedanib, we evaluated whether NK-mediated killing efficacy under treatment of nintedanib would be improved in a cancer-CAF mixed spheroid coculture. Using a 3D coculture system, we investigated the direct cytotoxic activity of NK cells (figure 3A,B). Interestingly, we observed that at an effector (E) to target (T) ratio of 0.5:1, the time-course experiments showed a robust NK-driven cancer killing effect when combined with nintedanib treatment (figure 3A). We also confirmed the inhibitory effects on CAFs in the presence of nintedanib (figure 3B). Without NK92 cells, there was no cancer killing, even in the presence of nintedanib (figure 3C). Moreover, the total number of NK cells did not change after NK-mediated killing (online supplemental figure S4). Mono or double spheroids were used as a control (figure 3D–F and online supplemental figure S4). We also measured annexin V influx in the dead cells of GFP-Capan2 (online supplemental figure S4).

Next, we found that nintedanib alone did not affect the NK cell activities because of no differences in the expression of natural cytotoxicity receptors such as NKp30, NKp44, and NKp46 and the activating marker CD69 in NK92 cells (figure 3G and online supplemental figure S5). We reason that NK cells had a low expression of PDGFRβ, leading to a lower inhibitory signal of nintedanib in NK cells (online supplemental figure S6). However, nintedanib influenced NK92 cells in the 3D cocultured cells. We noticed that NK cell-activating receptors were significantly upregulated on NK92 cells in the presence of nintedanib beyond exerting their cytotoxic function (figure 3H and online supplemental figure S5). Similarly, we found that peripheral blood mononuclear cell-derived NK (PBNK) cells exhibited an enhanced NK cytotoxic function and activation in the presence of nintedanib (figure 3I,J and online supplemental figure S7).

Conditioned media from nintedanib-treated CAFs rescued functional impairment of NK cells via a significant reduction of CAF-secreted IL-6

To reveal the underlying mechanism of the effect of nintedanib on the NK-promoting function in the NK-spheroid cocultures only, we assessed the impact of nintedanib-treated conditioned media (CM) on PBNK cells alone. We observed that the expression of activating receptors, such as DNAX accessory molecule (DNAM-1, CD226), NKp30, NKp44, NKp46, and NKG2D was elevated on nintedanib-treated CM (figure 4A). Consequently, the impaired NK function was rescued with enhanced NK-mediated cytolysis (figure 4B). Next, we analyzed the CAF-released secretome relative to CAF-mediated immunoregulatory functions. We found that CAFs released large amounts of cytokines and growth factors in the control, whereas treatment with nintedanib particularly inhibited the release of cytokines, such as IL-6 and IL-8, and growth factors, such as PDGF receptor/ligands (online supplemental figure S8) and figure 4C,D). Among them, we observed a strong reduction in CAF-released IL-6 in the presence of nintedanib, inferring the potential role of IL-6 in NK dysfunction (figure 4C). Consistent with the reduced secretion of IL-6, the level of both IL-6 mRNA and protein was significantly decreased in response to treatment with nintedanib in CAFs (figure 4E,F). We also found that PDGF ligands, such as PDGF-AB and PDGF-BB that bind to PDGFRβ, induced the secretion of IL-6 in CAFs, confirming the molecular target of nintedanib (figure 4G).

Next, we examined the relation between the CAF-derived production of IL-6 and NK cell dysfunction, and tested the impact of IL-6 in cancer or NK cells. We stably generated NanoLuc luciferase-expressing Capan2 (Capan2-Luc) cells for a luminescence-based tumor killing assay. Despite no differences in the viability of Capan2-Luc cells alone, the exogenously IL-6-pretreated NK cells impeded their tumor killing efficacies (figure 5A–C). We further confirmed that blockade of IL-6 using anti-IL-6 antibody in nintedanib-treated CM in NK cells prior to coculture significantly enhanced the expression of NK activating receptors, such as NKp30, NKp46, NKG2D and DNAM-1 (figure 5D). Thus, we concluded that CAF-derived IL-6 trans-signaling attenuated the activation of NK cells. We further identified that direct treatment of IL-6 in PBNK induced activation of STAT3, rather than AKT and ERK (figure 5E), whereas the addition of anti-IL-6 antibody led to inhibition of pSTAT3 (figure 5E). Additionally, anti-IL-6 antibody-treated CM or nintedanib-treated CM inhibited activation of STAT3 signaling on PBNK cells

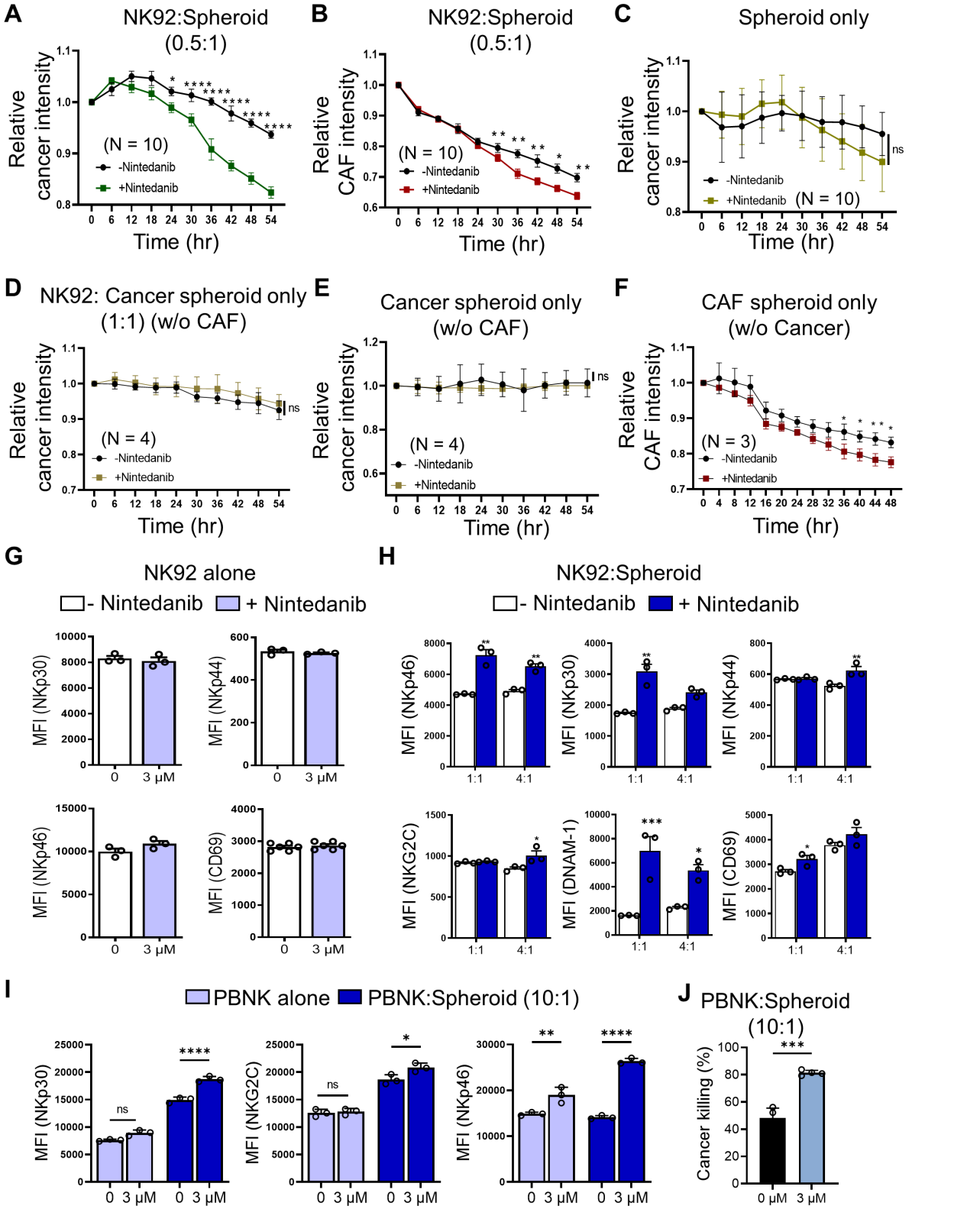

Figure 3 Nintedanib improved the NK-mediated cancer killing through the upregulated activation of markers. (A, B) To test the effect of nintedanib on NK-driven cytolysis, NK92 cells were incubated in the Capan2-CAF spheroid system with or without 3 μM nintedanib, and the relative intensities were measured in a time-dependent course based on fluorescence live cell imaging. (C) Cancer-CAF spheroids only, in the presence or absence of nintedanib. (D–F) Each single cell-type spheroid with or without NK92 was used as a control. (G–J) The direct or indirect effect of nintedanb on NK cytotoxic function was evaluated according to coculturing condition. Incubation with NK92 (G, H) and primary NK cells (I, J), respectively. Nintedanib ameliorated the function of NK cells only in Capan2-CAF spheroid condition. P values were determined using one-way ANOVA followed by multiple comparison test. *p<0.05, **p<0.01, ***p<0.001, ****p<0.0001. ANOVA, analysis of variance; CAF, cancer-associated fibroblast; NK, natural killer.

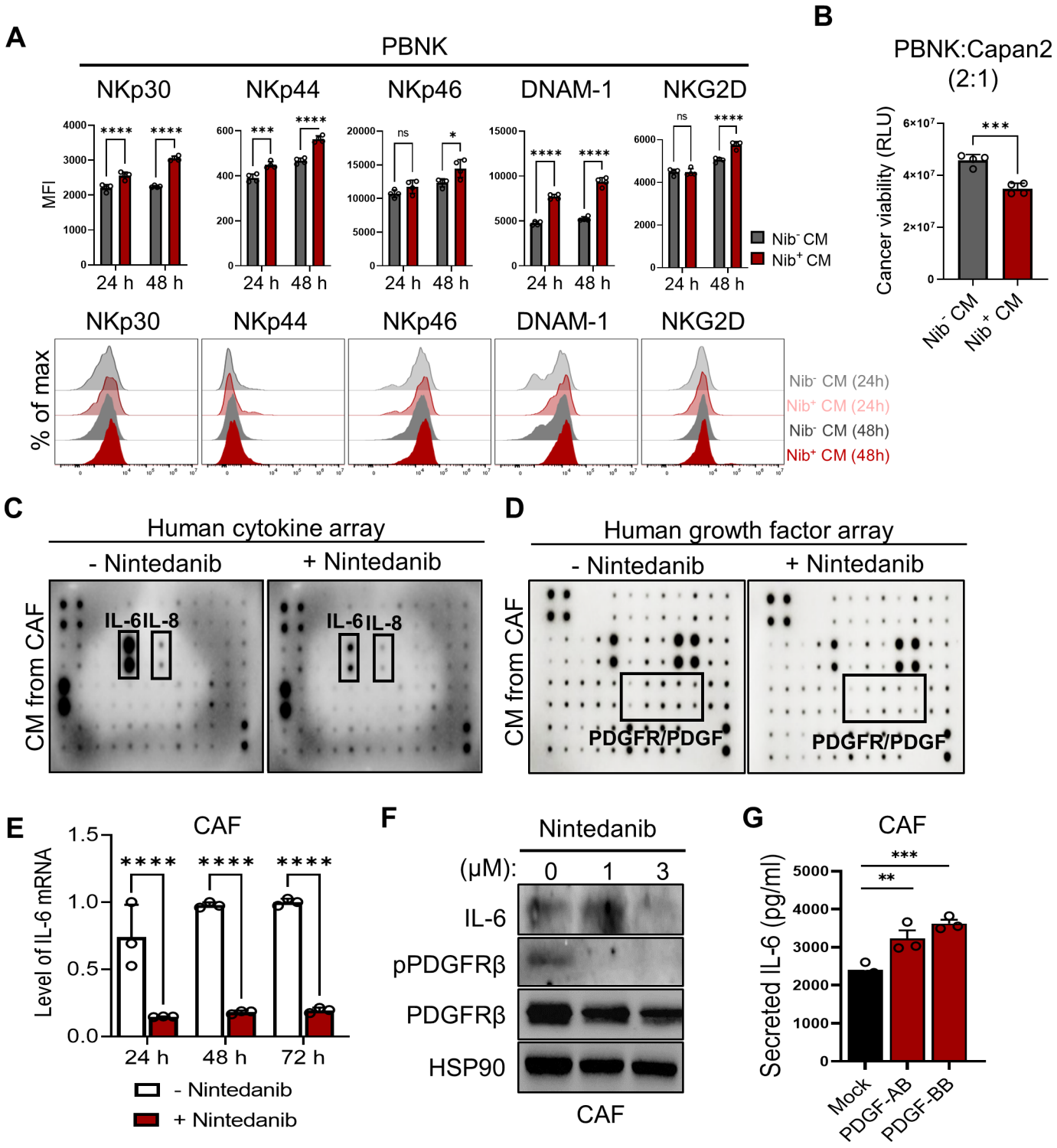

Figure 4 Nintedanib-treated CAFs exhibited a significant reduction in CAF-derived IL-6, consequently rescuing NK inhibition. (A, B) To reveal a NK-promoting role on treatment with nintedanib (Nib), the impact of nintedanib-treated condition media (CM) was evaluated through the expression of NK activating markers (A) or NK-mediated killing efficacy (B), respectively. p values were determined using one-way ANOVA followed by multiple comparison test. *p<0.05, **p<0.01, ***p<0.001, ****p<0.0001. Quantitative data were obtained from N=4 per each group. (C, D) Human cytokine array (C) and growth factor array (D), respectively, were conducted in the presence or absence of nintedanib to analyze the CAF-released secretome. (E, F) The level of IL-6 mRNA (****p<0.0001.) (E) or protein (F) is shown under treatment with nintedanib in CAFs. (G) Stimulation of PDGF ligands, such as PDGF-AB and PDGF-BB in CAFs induced the secretion of IL-6. Quantitative data were obtained from N=3 per each group. (**p<0.01, ***p<0.001) ANOVA, analysis of variance; CAF, cancer-associated fibroblast; NK, natural killer; PBNK, peripheral blood mononuclear cell-derived NK; PDGF, platelet-derived growth factor.

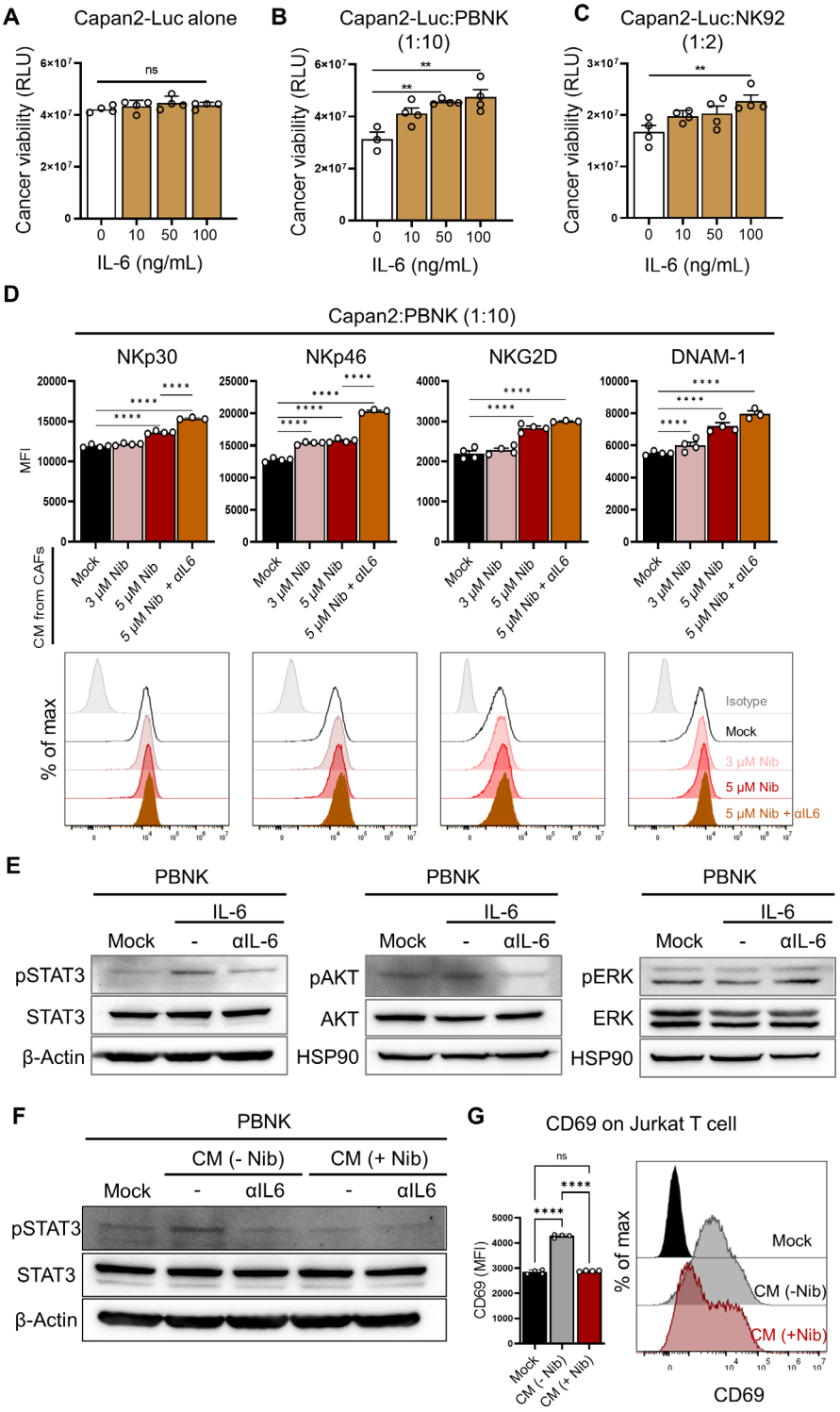

Figure 5 CAF-secreted IL-6 impeded NK cytotoxic function. (A–C) The effect of exogenous treatment with IL-6 in Capan2-Luc cells alone (A) and in coculture of Capan2-Luc with PBNK (B) or NK92 (C). For the luminescence-based tumor killing assay, nanoLuc luciferase-expressing Capan2 (Capan2-Luc) cells were generated. (**p<0.01) (B, C) PBNK or NK92 cells were cocultured with Capan2-Luc cells at a 10:1 or 2:1 ratio for 24 hours. (****p<0.0001) (D) The effect of the suppression of IL-6 on the activation of NK cells was investigated in the coculture of Capan2 with PBNK. Prior to coculture, PBNK cells were pretreated with CM from mock-, nintedanib-, and nintedanib plus αIL-6-treated CAFs for 24 hours. CAF-derived IL-6 attenuated the activation of NK cells. (E) IL-6-mediated signal transduction pathways in PBNK were validated under the treatment of IL-6 (100 ng/mL) with or without anti-IL-6 antibody (100 ng/mL) for 2 hours. (F) PBNK cells in the presence or absence of αIL-6 were incubated with CM from mock-, and nintedanib-treated CAFs for 2 h, and then the activation of STAT3 was detected by western blotting analysis. (G) Expression of CD69 on Jurkat T cells on treatment of CAF-derived CM in the presence or absence of nintedanib. Quantitative data were obtained from N=4 per group. (****p<0.0001) CAF, cancer-associated fibroblast; CM, conditioned media; NK, natural killer; PBNK, peripheral blood mononuclear cell-derived NK.

(figure 5F). To confirm the effect of IL-6 on NK cells, we evaluated the expression of IL-6 receptors, including IL-6Rα (CD126) and gp130 (CD130), on NK cells responsible for IL-6 signaling transduction (online supplemental figure S9).[37] IL-6 binds to membrane-bound IL-6Rα or soluble IL-6Rα, and subsequently binds to the signal transduction receptor subunit gp130, triggering IL-6-induced signaling activation.[38] Based on flow cytometry analysis, gp130 was ubiquitously expressed on NK, cancer, and CAFs; however, expression of IL-6Rα was limited to a small population of NK cells (online supplemental figure S9). Notably, it is necessary to measure soluble IL-6Rα from cell culture media, being generated using alternative RNA splicing or proteolytic cleavage. Taken together, the suppression of CAF-derived IL-6 via treatment with nintedanib might rescue the impairment of NK cytotoxic function by elevating the expression of NK activating receptors following the suppression of STAT3 signaling. Next, we tested the impact of IL-6 signaling on Jurkat T cells for broad therapeutic application of IL-6 blockade (figure 5G). Notably, CAF-derived CM induced CD69 as an activation marker on Jurkat T cells, while nintedanib-treated CM inhibited CD69 activation. Further investigations are required to determine the clinical impacts of IL-6 blockers on primary T cells.

Nintedanib triggered the synergistic cytotoxicity of MSLN-targeted CAR-NK against MSLN-positive PDAC

To maximize the synergistically therapeutic combination of nintedanib against PDAC, we first generated CAR-NK cells targeting MSLN-positive Capan2 cancer cells. For synergistic therapeutic combination of CAR-NK, we chose MSLN as a promising tumor antigen. MSLN is highly expressed in several solid neoplasmas, including pancreatic cancer, and its selective expression on malignant cells indicates a promising biomarker for targeted therapy.[39 40] First, we confirmed that only low expression of MSLN was observed in CAFs by flow cytometry analysis (online supplemental figure S10). For targeting the MSLN tumor antigen, we introduced a 4-1BB (CD137; TNFRSF9)-dependent second generation of CAR construct carrying murine SS1 scFv into NK92 cells.[40 41] We then validated the MSLN-dependent tumor killing efficacy of CAR-NK cells using FACS and live cell imaging (online supplemental figure S11). To optimize the in vitro NK-mediated cytotoxic function, we added nintedanib in the coculture of MSLN-targeted CAR-NK and spheroids (2:1; figure 6A,B). As expected, treatment with nintedanib significantly induced the CAR-NK-mediated cytotoxic function in vitro. Prior to therapeutic studies, we generated an in vivo tumor xenograft model, in which luciferase-overexpressing Capan2 cells were subcutaneously injected in the presence or absence of CAFs (online supplemental figure S12). Due to the limited availability of the orthotopically implanted cancer-bearing mice model, we generated a cancer:CAF mixed xenograft tumor via subcutaneous injection of cancer/CAF mixture cells to investigate the effect of CAFs in vivo.[42] We observed that the Capan2-Luc:CAF-mixed xenograft tumor exhibited higher proliferation compared with the Capan2 alone xenograft tumor, implying the tumor-promoting effects of CAFs. Consistent with the observation in our in vitro functional tests, combinatory treatment with nintedanib achieved synergistic cytotoxic effects of CAR-NK in Capan2-Luc:CAF-mixed xenograft mice (figure 6C–F and online supplemental figure S13). Notably, we found that treatment of CAR-NK without nintedanib did not suppress tumor growth in vivo, preserving the dysfunction of CAR-NK in CAF-rich solid tumors (figure 6D,E). However, 34 days after treatment, combination-treated tumors seemed to recur; however, the optimal tumor reduction in the combinatory treatment group was confirmed (figure 6D,E). Thus, combinatory-treated tumors were excised for further investigation in ex vivo experiments when optimal tumor reduction was reached. We noticed that nintedanib-treated groups had significantly reduced CAF populations in H&E-stained tumor sections, which positively correlated with the expression of PDGFRβ (online supplemental figure S13). In addition, tumor-infiltrating CAR-NK cells were highly increased in the nintedanib-treated tumor sections, resulting in the acquired loss of the expression of MSLN due to CAR-NK-mediated tumor killing (figure 6F and online supplemental figure S13). Next, we evaluated off-target toxicity through observation of histological changes in dissected normal organs or measurement of various blood parameters, all of which showed no significant differences between groups (online supplemental figure S14).

Next, we examined PBNK-derived CAR (CAR-PBNK)-mediated cancer killing using patient-derived or cancer cell line-derived organoids that are suitable for clinical study of CAR-NK. To mimic the patient TME within organoids, we established patient (Og-AMC-363)- or cancer cell line (AsPC1_XO)-derived organoid/CAF co-culture systems by adding patient-derived CAFs (online supplemental figure S15). We assessed CAR-PBNK-mediated cancer killing on nintedanib treatment using a mCherry-expressing patient-derived organoid/CAF co-culture system (figure 6G). Consistent with the observations in the in vivo experiment, nintedanib treatment reinforced CAR-PBNK-mediated cancer killing in the organoid/CAF co-culture system. To further confirm the therapeutic effect on IL-6 signaling inhibition for NK-based immunotherapy, we investigated the efficacy of CAR-PBNK cells with co-treatment of IL-6R blocking antibody (tocilizumab), which binds to the soluble and transmembrane form of IL-6Rs.[43] To test the potential of an alternative combination IL-6R blocking antibody (tocilizumab) treatment for synergistic CAR-NK-mediated cancer killing, tocilizumab was co-incubated with CAR-PBNK cells in the organoid/CAF co-culture system (online supplemental figure S16). Remarkably, the combinatory treatment with tocilizumab exhibited a significant increase in CAR-NK-mediated killing. Thus, NK-based immunotherapy with IL-6 blockade suggests a promising therapeutic strategy for effective cancer treatment.

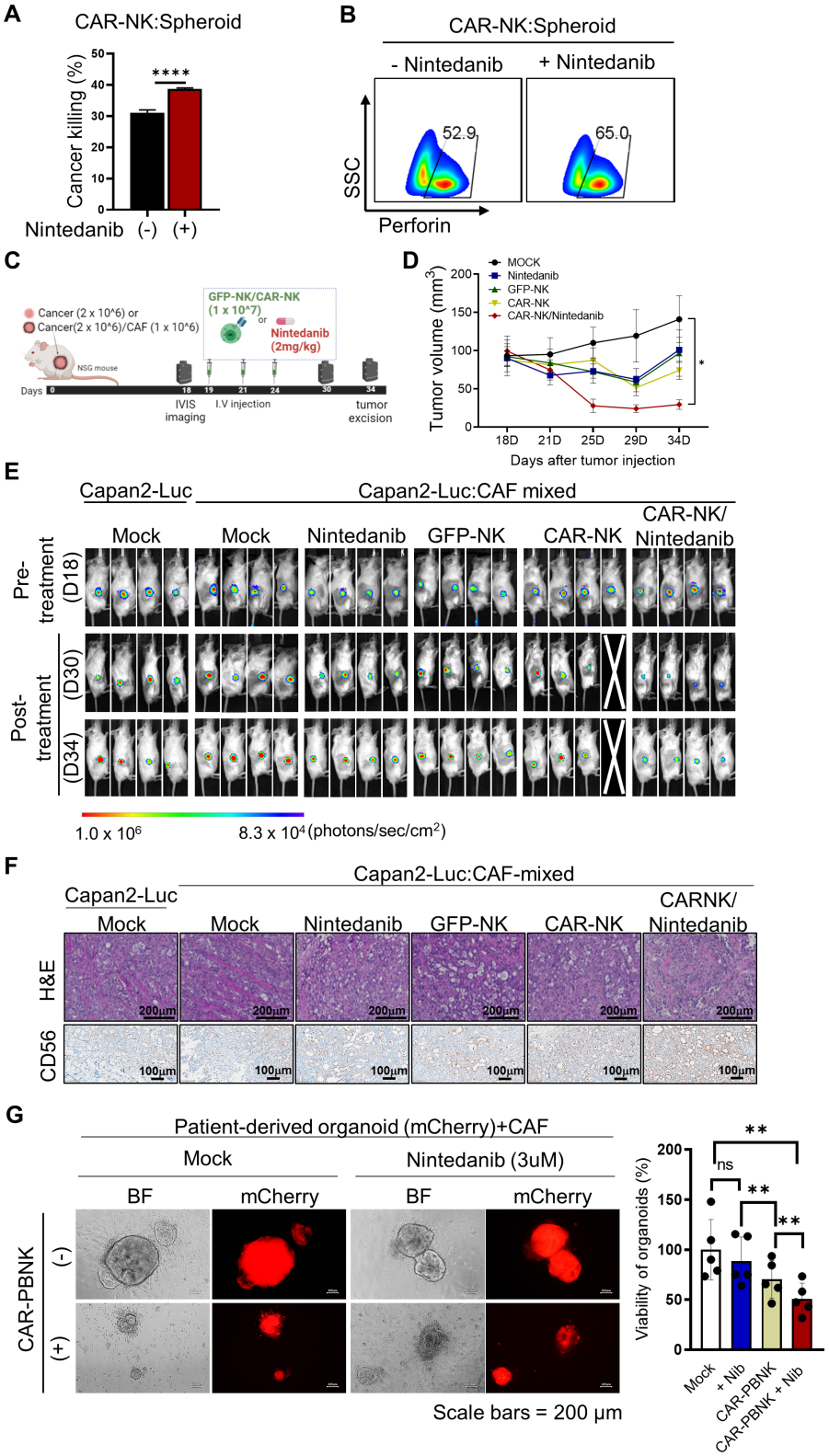

Figure 6 Optimal combination of MSLN-CAR-NK and nintedanib exhibited significant tumor killing in vitro and in vivo. (A, B) The CAR-NK-mediated cytotoxic function was significantly enhanced against MSLN-positive Capan2 under treatment with nintedanib (N=3). (****p<0.0001) (C) The scheme of the in vivo experiment for the combination of CAR-NK and nintedanib. For therapeutic studies, Capan2-Luc alone or a mixture of Capan2-Luc and CAF was subcutaneously injected into mice. (D, E) For therapeutic evaluation, the growth of each tumor (N=4) was monitored through size measurement using a caliper (*p<0.05) (D) or through visualization of the in vivo luminescence signal using the IVIS spectrum imaging system (E). (F) Histological analysis and IHC staining were conducted in excised tumor sections. (**p<0.01) (G) Synergistic cancer effect of CAR-PBNK with nintedanib, based on a patient-derived organoid/CAF co-culture system. CAF, cancer-associated fibroblast; CAR, chimeric antigen receptor; MSLN, mesothelin; NK, natural killer; IHC, immunohistochemical.

The expression of MSLN positively correlated with the PDGFRβ-positive population area, while the combination of the expression of MSLN and PDGFRβ$^+$ CAFs was associated with poor clinical outcomes

We investigated the potential associations between MSLN and PDGFRβ for a potential combinatorial immunotherapy. We performed immunohistochemistry (IHC) staining to score the expression of MSLN and PDGFRβ in normal and PDAC tumor sections, respectively (online supplemental figure S17 and figure 7A). Based on IHC staining, we evaluated the association of MSLN and PDGFRβ with clinical outcomes in patients with PDAC (figure 7B and online supplemental tables S2,S3).

We found that the MSLN-high group of tumors was significantly associated with inferior overall survival (OS). However, neither the PDGFRβ-high group nor the combination-high group was associated with promising survival outcomes. We observed similar survival rates when we used public transcriptomic data from the Cancer Genome Atlas (TCGA; online supplemental figure S18). Nintedanib directly inhibited phosphorylation of PDGFRβ, resulting in cell death in CAFs. Thus, we speculated that the PDGFRβ-positive area within the TME might be associated with poor survival outcomes rather than the expression degree of PDGFRβ. Subsequently, we analyzed the percentage of the PDGFRβ-positive population area occupied within the TME, but not based on the intensity of the expression of PDGFRβ (figure 7C). We detected that PDGFRβ PA varied widely from 0.57% to 32.67% between 43 patient-derived tumor sections, and was classified into a low or high group according to the area percentage (%; figure 7C and online supplemental table S3). Importantly, we found that the combination of the expression of MSLN and PDGFRβ PA exhibited a significantly lower OS with unfavorable clinical outcomes (figure 7D). According to our observation (figure 4C) of strong secretion of IL-6 from PDGFRβ-positive CAFs, we further tested the clinical association of IL-6 or the combination of MSLN and IL-6 in patient-derived tumor sections. Interestingly, based on the PA of IL-6, IL-6 PA alone and the combination of IL-6 PA with MSLN within the TME were positively associated with poor survival (figure 7E–G). TCGA data also showed that IL-6 at the RNA level was significantly associated with poor survival outcomes (online supplemental figure S18).

We further performed IHC staining on patient-derived tumor sections diagnosed with liver and gastric cancer (online supplemental figure S19). Interestingly, both MSLN and PDGFRβ were strongly detected on gastric tumor sections (online supplemental figure S19). Thus, this combination can serve as a potential prognostic or therapeutic marker for the treatment of PDAC or other solid tumors (online supplemental figure S20).

DISCUSSION

PDGF-PDGFR axis signals are implicated in the progress of diverse diseases. PDGFs, as a family of four cysteine-knot-type growth factors (PDGF-A, PDGF-B, PDGF-C, and PDGF-D) are potent mitogens that control the proliferation and survival of cancer cells and fibroblasts.[44 45] Isoforms of PDGF bind to two receptors, PDGFRα and PDGFRβ, inducing different homodimeric and heterodimeric complexes, which in turn exert multiple downstream signaling.[45 46] Autocrine PDGF-induced signaling is activated in certain type of carcinomas, such as gliomas, sarcoma and leukemia, whereas paracrine activation of cancer-derived PDGFs triggers the recruitment of stromal cells, such as fibroblasts and vascular endothelial cells.[46] Notably, cancer-secreted PDGF-BB contributes to stromal resistance by protecting fibroblasts from hydrogen peroxide-dependent cell damage.[47] Furthermore, the degree of CAF infiltration has been strongly correlated with the strength of PDGF-PDGFR axis-mediated signal transduction.[48] Thus, the PDGF-PDGFR axis is an important regulator in TME modulation, serving as a promising therapeutic target for cancer treatment. In this study, we demonstrated that nintedanib, as an antifibrotic drug, significantly inhibited the expression of pPDGFRβ in PDAC-derived CAFs via the PI3K/AKT and MAPK/ERK signaling pathways. Treatment with nintedanib led to a strong reduction in the secretion of IL-6, consequently causing cell death. Moreover, PDGF-AB or PDGF-BB induced the secretion of IL-6 in CAFs. In addition, nintedanib exhibited mild inhibitory effects on Capan2 cancer or NK cells alone. The differential effect of nintedanib according to cell type might be related to the level of expression of PDGFBRβ. Resting or IL-2-activated human NK cells express neither PDGFRα nor PDGFRβ. Indeed, on our IL-2 and IL-15-supplemented culture conditions, the surface expression of PDGFRβ was barely detectable in NK92 and PBNK cells. However, a recent study showed that IL-15-stimulated NK cells specifically induced the expression of PDGFRβ, contributing to long-term NK survival, which, however, did not affect the function of NK cells.[49] Taken together, further investigations regarding the expression of PDGFRβ in NK cells are needed for the development of effective cancer treatments through PDGFRβ-targeted CAFs.

In our study, we revealed that the expression of MSLN was positively correlated with the proportion of PDGFRβ$^+$ CAFs, and associated with unfavorable clinical outcomes. Reportedly, MSLN, a glycosylphosphatidylinositol-anchored cell surface glycoprotein is highly detectable in pancreatic cancers and various other tumors, while its expression is limited to normal mesothelial cells of the pleura, peritoneum, and pericardium.[40] The high expression of MSLN in tumors has been associated with poor clinical outcomes and shown to be involved in tumor cell proliferation, migration, and metastasis.[50] However, the expression of MSLN in human PDAC remains controversial, in that two studies revealed an association with unfavorable clinical outcomes.[51] However, another study showed no correlation with cancer aggressiveness.[39] In our study, 12 of 43 tumor sections had strong expression

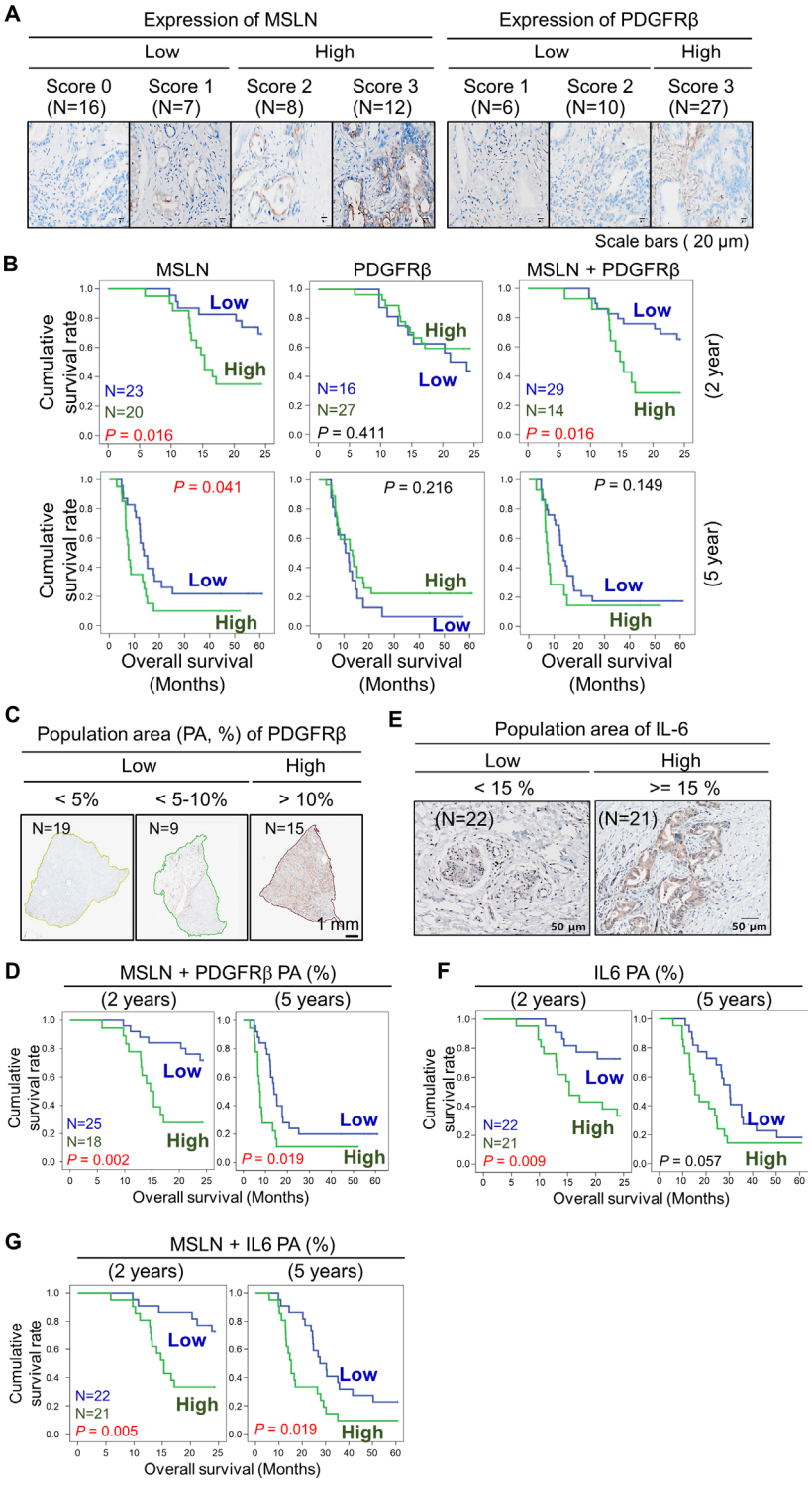

Figure 7 The combination of expression of MSLN and population of PDGFRβ$^+$ CAFs was associated with inferior clinical outcomes and poor overall survival (OS). (A) Based on IHC staining intensity, the expression score of MSLN and PDGFRβ was measured in patient-derived tumor sections. The degree of staining intensity was scored and sorted into a low or high group. (B) Analysis of OS according to the score of target expression. Survival rates were determined using the Kaplan-Meier method according to MSLN, PDGFRβ, and the combination of MSLN and PDGFRβ; MSLN-low (N=23), high (N=20); PDGFRβ-low (N=16), high (N=27); MSLN+PDGFRβ-low (N=29), high (N=14). (C) Using the vs200 research slide scanner, the PDGFRβ$^+$ population area (PA, %) was quantified and grouped into a low or high group; PDGFRβ PA-low (N=28), high (N=15). (D) Survival rates were analyzed according to the combination of MSLN and PDGFRβ PA; MSLN+PDGFRβ PA-low (N=25), high (N=18). (E) The IL-6 PA was quantified and grouped into a low and high group; IL-6 PA-low (N=22), high (N=21). (F) Analysis of OS according to the score of the IL-6 PA. (G) Survival rates were analyzed according to the combination of MSLN and IL-6 PA; MSLN+IL-6 PA-low (N=22), high (N=21). N indicates the number of clinical specimens. CAF, cancer-associated fibroblast; IHC, immunohistochemical; MSLN, mesothelin; PDGFRβ, platelet-derived growth factor receptor β.

of MSLN (score 3), and showed a significant association between MSLN positivity and reduced OS. In contrast, there was no relationship between the expression of PDGFRβ and clinical outcomes. Rather than PDGFRβ intensity scores, the combination of the degree of the PDGFRβ$^+$ PA and the expression of MSLN clearly exhibited inferior clinical outcomes, serving as a potential target of therapeutic interest.

In summary, we identified the novel combinatory immunotherapeutics of MSLN-targeted CAR-NK and nintedanib, which inhibited the proliferation of PDGFRβ$^+$ CAFs, eventually leading to enhanced CAR-NK cell infiltration, activation, and killing efficacy. Depletion of PDGFRβ$^+$ CAFs by treatment with nintedanib led to a significant reduction in CAF-secreted IL-6 through the ERK and AKT multiple signal pathways; in which paracrine IL-6 led to the abrogation of the NK cell-mediated cytotoxic function. Intriguingly, the IL-6-induced activation of STAT3 might function as an oncogenic pathway in NK cells, resulting in the reduced expression of NK activating receptors. Taken together, our therapeutic approach of combining MSLN-targeted CAR-NK and nintedanib might improve patient outcomes especially in stroma-rich cancers by efficiently modulating the TME.

Author affiliations
[1]Medicinal Materials Research Center, Biomedical Research Division, Korea Institute of Science and Technology, Seoul, Korea (the Republic of)
[2]Department of Life Sciences, College of Life Sciences and Biotechnology, Korea University, Seoul, Korea (the Republic of)
[3]Department of Convergence Medicine, Asan Institute for Life Sciences, University of Ulsan College of Medicine and Asan Medical Center, Seoul, Korea (the Republic of)
[4]Corporate Research & Development Center, UCI therapeutics, Seoul, Korea (the Republic of)
[5]Department of Pathology, Asan Medical Center, University of Ulsan College of Medicine, Seoul, Korea (the Republic of)
[6]Natural Product Research Center, Institute of Natural Products, Korea Institute of Science and Technology, Gangneung, Korea (the Republic of)
[7]Department of Health Sciences and Technology, Samsung Advanced Institute for Health Sciences and Technology (SAIHST), Sungkyunkwan University, Seoul, Korea (the Republic of)
[8]Department of Laboratory Medicine and Genetics, Samsung Medical Center, Sungkyunkwan University, Seoul, Korea (the Republic of)
[9]Division of Hepato-Biliary and Pancreatic Surgery, Department of Surgery, University of Ulsan College of Medicine, Asan Medical Center, Seoul, Korea (the Republic of)
[10]KHU-KIST Department of Converging Science and Technology, Kyung Hee University, Seoul, Korea (the Republic of)

Acknowledgements The authors thank the Asan Medical Center for their expert technical assistance with in vivo experiments.

Contributors MJ conceived the study. G-YG, YEL, TSK, JCK, and H-NY designed and performed the in vitro and in vivo experiments. MS cultured primary NK cells. EJ, S-MH, and EYK conducted a cohort study of patients. SCK established patient-derived CAFs. JHJ conducted organoid-based experiments. DC provided materials, including GE-feeder cells and a baboon envelope vector. MJ wrote the original draft. MJ, YEL, and EJ wrote the manuscript, with contributions and review by all other authors. MJ, EJ, and SCK accepts full responsibility for the work and/or the conduct of the study, had access to the data, and controlled the decision to publish.

Funding This work was supported by the National Research Foundation of Korea Grant funded by the Korean Government (grant number: 2020R1C1C1006421, 2020M3A9I4038662, and 2020M3A9I4038667) and by Korea Institute of Science and Technology (grant number: 2E32331 and 2V09550). This research was also supported by Korea Drug Development Fund funded by Ministry of Science and ICT, Ministry of Trade, Industry, and Energy, and Ministry of Health and Welfare (RS-2022-00166088, Republic of Korea). This study was supported by a grant (grant number: 2021IP0020-1) from Asan Institute for Life Sciences, Asan Medical Center. This work was also supported in part by Samsung Research Funding and Incubation Center of Samsung Electronics under Project Number SRFC-TC2003-02.

Competing interests None declared.

Patient consent for publication Not applicable.

Ethics approval This study complied with the Declaration of Helsinki and was reviewed and approved by the Institutional Review Board (IRB) of Asan Medical Center (IRB No. 2015-0480, 2018-0745, 2018-0710). Patients who underwent surgery for cancer were enrolled in this study, and informed consent was obtained before taking part in the study. Pancreatic, gastric, and liver cancer tissues that were pathologically diagnosed as carcinoma were delivered from the Bio-resource center (BRC No. 2018-13(167)).

Provenance and peer review Not commissioned; externally peer reviewed.

Data availability statement Data are available on reasonable request.

ORCID iD
Mihue Jang http://orcid.org/0000-0002-2135-2983

REFERENCES

1 Kleeff J, Korc M, Apte M, *et al*. Pancreatic cancer. *Nat Rev Dis Primers* 2016;2:16022.
2 Ligorio M, Sil S, Malagon-Lopez J, *et al*. Stromal microenvironment shapes the intratumoral architecture of pancreatic cancer. *Cell* 2019;178:160–75.
3 Chu GC, Kimmelman AC, Hezel AF, *et al*. Stromal biology of pancreatic cancer. *J Cell Biochem* 2007;101:887–907.
4 Jacobetz MA, Chan DS, Neesse A, *et al*. Hyaluronan impairs vascular function and drug delivery in a mouse model of pancreatic cancer. *Gut* 2013;62:112–20.
5 Olivares O, Mayers JR, Gouirand V, *et al*. Collagen-derived proline promotes pancreatic ductal adenocarcinoma cell survival under nutrient limited conditions. *Nat Commun* 2017;8:16031.
6 Hilmi M, Nicolle R, Bousquet C, *et al*. Cancer-associated fibroblasts: accomplices in the tumor immune evasion. *Cancers (Basel)* 2020;12:2969.
7 Knops AM, South A, Rodeck U, *et al*. Cancer-associated fibroblast density, prognostic characteristics, and recurrence in head and neck squamous cell carcinoma: a meta-analysis. *Front Oncol* 2020;10:565306.
8 Pereira BA, Vennin C, Papanicolaou M, *et al*. Caf subpopulations: a new reservoir of stromal targets in pancreatic cancer. *Trends Cancer* 2019;5:724–41.
9 Mhaidly R, Mechta-Grigoriou F. Role of cancer-associated fibroblast subpopulations in immune infiltration, as a new means of treatment in cancer. *Immunol Rev* 2021;302:259–72.
10 Linares J, Marín-Jiménez JA, Badia-Ramentol J, *et al*. Determinants and functions of cafs secretome during cancer progression and therapy. *Front Cell Dev Biol* 2020;8:621070.
11 Moncada R, Barkley D, Wagner F, *et al*. Integrating microarray-based spatial transcriptomics and single-cell RNA-seq reveals tissue architecture in pancreatic ductal adenocarcinomas. *Nat Biotechnol* 2020;38:333–42.

12 Hosein AN, Huang H, Wang Z, *et al*. Cellular heterogeneity during mouse pancreatic ductal adenocarcinoma progression at single-cell resolution. *JCI Insight* 2019;5:e129212.
13 Elyada E, Bolisetty M, Laise P, *et al*. Cross-species single-cell analysis of pancreatic ductal adenocarcinoma reveals antigen-presenting cancer-associated fibroblasts. *Cancer Discov* 2019;9:1102–23.
14 Ohlund D, Handly-Santana A, Biffi G, *et al*. Distinct populations of inflammatory fibroblasts and myofibroblasts in pancreatic cancer. *J Exp Med* 2017;214:579–96.
15 Boyd LNC, Andini KD, Peters GJ, *et al*. Heterogeneity and plasticity of cancer-associated fibroblasts in the pancreatic tumor microenvironment. *Semin Cancer Biol* 2022;82:184–96.
16 Biffi G, Oni TE, Spielman B, *et al*. Il1-Induced JAK/STAT signaling is antagonized by TGFβ to shape CAF heterogeneity in pancreatic ductal adenocarcinoma. *Cancer Discov* 2019;9:282–301.
17 Guerra N, Tan YX, Joncker NT, *et al*. NKG2D-deficient mice are defective in tumor surveillance in models of spontaneous malignancy. *Immunity* 2008;28:571–80.
18 Imai K, Matsuyama S, Miyake S, *et al*. Natural cytotoxic activity of peripheral-blood lymphocytes and cancer incidence: an 11-year follow-up study of a general population. *Lancet* 2000;356:1795–9.
19 Shimasaki N, Jain A, Campana D. Nk cells for cancer immunotherapy. *Nat Rev Drug Discov* 2020;19:200–18.
20 Curti A, Ruggeri L, Parisi S, *et al*. Larger size of donor alloreactive NK cell repertoire correlates with better response to NK cell immunotherapy in elderly acute myeloid leukemia patients. *Clin Cancer Res* 2016;22:1914–21.
21 Li T, Yang Y, Hua X, *et al*. Hepatocellular carcinoma-associated fibroblasts trigger NK cell dysfunction via PGE2 and IDO. *Cancer Lett* 2012;318:154–61.
22 Sun C, Sun H, Zhang C, *et al*. Nk cell receptor imbalance and NK cell dysfunction in HBV infection and hepatocellular carcinoma. *Cell Mol Immunol* 2015;12:292–302.
23 Huang H, Zhang Y, Gallegos V, *et al*. Targeting TGFβr2-mutant tumors exposes vulnerabilities to stromal TGFβ blockade in pancreatic cancer. *EMBO Mol Med* 2019;11:e10515.
24 Geng X, Chen H, Zhao L, *et al*. Cancer-associated fibroblast (CAF) heterogeneity and targeting therapy of cafs in pancreatic cancer. *Front Cell Dev Biol* 2021;9:655152.
25 Kraman M, Bambrough PJ, Arnold JN, *et al*. Suppression of antitumor immunity by stromal cells expressing fibroblast activation protein-alpha. *Science* 2010;330:827–30.
26 Duperret EK, Trautz A, Ammons D, *et al*. Alteration of the tumor stroma using a consensus DNA vaccine targeting fibroblast activation protein (FAP) synergizes with antitumor vaccine therapy in mice. *Clin Cancer Res* 2018;24:1190–201.
27 Loeffler M, Krüger JA, Niethammer AG, *et al*. Targeting tumor-associated fibroblasts improves cancer chemotherapy by increasing intratumoral drug uptake. *J Clin Invest* 2006;116:1955–62.
28 Lo A, Wang L-CS, Scholler J, *et al*. Tumor-Promoting desmoplasia is disrupted by depleting FAP-expressing stromal cells. *Cancer Res* 2015;75:2800–10.
29 Feig C, Jones JO, Kraman M, *et al*. Targeting CXCL12 from FAP-expressing carcinoma-associated fibroblasts synergizes with anti-PD-L1 immunotherapy in pancreatic cancer. *Proc Natl Acad Sci U S A* 2013;110:20212–7.
30 Kolb P, Upagupta C, Vierhout M, *et al*. The importance of interventional timing in the bleomycin model of pulmonary fibrosis. *Eur Respir J* 2020;55:1901105.
31 Hilberg F, Roth GJ, Krssak M, *et al*. Bibf 1120: triple angiokinase inhibitor with sustained receptor blockade and good antitumor efficacy. *Cancer Res* 2008;68:4774–82.
32 Richeldi L, Costabel U, Selman M, *et al*. Efficacy of a tyrosine kinase inhibitor in idiopathic pulmonary fibrosis. *N Engl J Med* 2011;365:1079–87.
33 Borie R, Fabre A, Prost F, *et al*. Activation of somatostatin receptors attenuates pulmonary fibrosis. *Thorax* 2008;63:251–8.
34 Tug T, Kara H, Karaoglu A, *et al*. The effect of octreotide, an analog of somatostatin, on bleomycin-induced interstitial pulmonary fibrosis in rats. *Drug Chem Toxicol* 2013;36:181–6.
35 Cheng D, Xu Q, Wang Y, *et al*. Metformin attenuates silica-induced pulmonary fibrosis via AMPK signaling. *J Transl Med* 2021;19:349.
36 Li S-X, Li C, Pang X-R, *et al*. Metformin attenuates silica-induced pulmonary fibrosis by activating autophagy via the AMPK-mtor signaling pathway. *Front Pharmacol* 2021;12:719589.
37 Hibi M, Murakami M, Saito M, *et al*. Molecular cloning and expression of an IL-6 signal transducer, gp130. *Cell* 1990;63:1149–57.
38 Reeh H, Rudolph N, Billing U, *et al*. Response to IL-6 trans- and IL-6 classic signalling is determined by the ratio of the IL-6 receptor α to gp130 expression: fusing experimental insights and dynamic modelling. *Cell Commun Signal* 2019;17:46.
39 Le K, Wang J, Zhang T, *et al*. Overexpression of mesothelin in pancreatic ductal adenocarcinoma (PdaC). *Int J Med Sci* 2020;17:422–7.
40 Lv J, Li P. Mesothelin as a biomarker for targeted therapy. *Biomark Res* 2019;7:18.
41 Kelly RJ, Sharon E, Pastan I, *et al*. Mesothelin-targeted agents in clinical trials and in preclinical development. *Mol Cancer Ther* 2012;11:517–25.
42 Hutton C, Heider F, Blanco-Gomez A, *et al*. Single-cell analysis defines a pancreatic fibroblast lineage that supports anti-tumor immunity. *Cancer Cell* 2021;39:1227–44.
43 Tanaka T, Narazaki M, Kishimoto T. Interleukin (IL-6) immunotherapy. *Cold Spring Harb Perspect Biol* 2018;10:a028456.
44 Bartoschek M, Pietras K. Pdgf family function and prognostic value in tumor biology. *Biochem Biophys Res Commun* 2018;503:984–90.
45 Heldin CH. Targeting the PDGF signaling pathway in tumor treatment. *Cell Commun Signal* 2013;11:97.
46 Andrae J, Gallini R, Betsholtz C. Role of platelet-derived growth factors in physiology and medicine. *Genes Dev* 2008;22:1276–312.
47 Werth C, Stuhlmann D, Cat B, *et al*. Stromal resistance of fibroblasts against oxidative damage: involvement of tumor cell-secreted platelet-derived growth factor (PDGF) and phosphoinositide 3-kinase (PI3K) activation. *Carcinogenesis* 2008;29:404–10.
48 Tejada ML, Yu L, Dong J, *et al*. Tumor-Driven paracrine platelet-derived growth factor receptor alpha signaling is a key determinant of stromal cell recruitment in a model of human lung carcinoma. *Clin Cancer Res* 2006;12:2676–88.
49 Ma S, Tang T, Wu X, *et al*. PDGF-D-pdgfrβ signaling enhances IL-15-mediated human natural killer cell survival. *Proc Natl Acad Sci U S A* 2022;119:e2114134119.
50 Hilliard TS. The impact of mesothelin in the ovarian cancer tumor microenvironment. *Cancers (Basel)* 2018;10:277.
51 Einama T, Kamachi H, Nishihara H, *et al*. Co-Expression of mesothelin and CA125 correlates with unfavorable patient outcome in pancreatic ductal adenocarcinoma. *Pancreas* 2011;40:1276–82.